Two-step migration of particles in evaporating bimodal suspension films at high Peclet numbers

Two-step migration of particles in evaporating bimodal suspension films at high Peclet numbers

Tomonori TASHIMA and Masato YAMAMURA*

Department of Applied Chemistry, Kyushu Institute of Technology, Fukuoka, Japan, 804-8550

* Email of corresponding author: yamamura@che.kyutech.ac.jp

Abstract:

During the drying of bimodal colloidal suspensions containing particles with various sizes, smaller particles preferentially migrate to the top surface under particular drying conditions, leading to show undesirable drying defects in batteries and in other coating applications. Despite extensive previous studies, the migration mechanism is far from understood because few *in-situ* observations are available to support the hypotheses. To remedy this, we use *real-time* photoluminescence (PL) microscopy to investigate the migration of small fluorescent latex particles co-dispersing with large nonemissive latex particles. Comparing the measured PL intensity with that predicted by a model allows us to determine the quantity of small particles near the evaporating surface. The results reveal that the fluorescent particles segregate in two-steps: the primary segregation occurs early in the evaporation stage, whereas the secondary stepwise migration occurs when the air-liquid interface invades the particle consolidation layer. The latter migration is attributed to the flow-induced motion of small particles that move through interstitial spaces between large particles.

Keywords: suspension, drying, coating, migration, photoluminescence

Introduction

As a particulate coating dries, particle-concentration gradients develop through the coating. For example, consider a gas-diffusion-limited drying stage, in which the free surface descends toward the substrate with a constant velocity E. Evaporation can cause particles to accumulate and bring them into close packing at the free surface when the descending motion of the surface is much faster than the thermal Brownian diffusion of particles with velocity V_D [1]. The dimensionless Peclet number, $Pe = E/V_D$, characterizes the kinetic balance between these two motions [2]. Surface segregation of particles occurs for $Pe >> 1$, whereas the particles maintain a homogeneous distribution for $Pe << 1$.

Secondary particle segregation has been reported to occur in the late drying stages of bimodal suspensions evaporating at high *P*e [3-6]. For blends of charged/uncharged particles, for instance, the charged particles repel from the liquid/air interface via electrostatic repulsion, resulting in a preferential enrichment of uncharged particles at the free surface, as verified experimentally [4] and numerically [5]. However, in bimodal suspensions that contain particles of varying sizes, Luo et al. (2008) focused on the role of the liquid/air interface that retreats into the particle packing, and postulated that a decreased pressure of the liquid beneath the curved menisci could initiate a flow that transports nanoparticles through interstitial spaces between larger particles [3]. Such a preferential segregation behavior is not expected from the competition between the evaporation-induced accumulation and diffusion-induced homogenization, because either particle could primarily co-segregate at the free surface if its Peclet number much exceeds unity.

Understanding the "two-step" evolution in concentration gradients in bimodal suspensions requires *in-situ* quantification of the distribution of each particle across the coating thickness. Despite the extensive previous investigations using NMR imaging [7], ellipsometry [8], cryogenic scanning electron microscopy (Cryo-SEM) [1, 9], and numerical modeling [10], few studies have directly captured the onset of secondary particle segregation. Recently, cross-sectional Raman spectroscopy [11] and energy-dispersive x-ray spectroscopy (EDS) [12] have shed light on the underlying physics by determining local compositions in graphite-polymer particulate electrodes. However, the dynamics in the particle consolidation layer across the coating remain unknown because of limited spatial resolution. To the best of our knowledge, the precise mechanism behind preferential surface segregation of smaller particles in bimodal suspensions remains a subject of ongoing debate.

In the present study, we use *real-time* photoluminescence (PL) microscopy to investigate the preferential migration of small fluorescent latex particles co-dispersing with large nonemissive latex particles, particularly for drying at high Peclet numbers. The small latex particles exhibit photoluminescence in liquids when excited (e.g., by laser irradiation through the whole coating). The PL technique can be applied to particulate coatings without any sophisticated sample preparation, which is a great advantage over other measurement techniques. To quantify the distribution of particles, we developed a one-dimensional optical emission/absorption model to predict the transient PL intensity during evaporation. The measured and predicted PL intensities are consistent.

Experimental Methods and Materials

We used fluorescent polystyrene latex particles (micromer®-redF, micromod, Germany; diameter = 100 nm; zeta potential in water = – 40 ± 5 mV) and nonemissive polystyrene latex particles (micromer®, micromod, Germany; diameter = 200 nm or 8 μm). Blended suspensions were prepared from the small and large latex particles. The maximum excitation and emission wavelengths of the

fluorescent particle are 552 and 580 nm, respectively. Sodium carboxymethyl cellulose (CMC, Dai-ichi Kogyo Seiyaku, Japan) was used as a water-soluble polymer. The average molecular weight and the degree of substitution of CMC were 180,000–190,000 g/mol and 0.65–0.75, respectively. The CMC aqueous solution was added to the latex suspensions, and mixed for 12 h to obtain coating liquids. The preliminary transmittance spectroscopy shows that the light absorption coefficient of CMC is negligibly small at the wavelength range of interest (λ = 500 ~ 600 nm), which indicates that the polymer is optically transparent and does not influence the PL measurement described below.

Figure 1 shows a schematic of the drying apparatus. A TEM00-mode laser (LasirisTM Green, Coherent, USA; wavelength = 532 ± 1 nm) was incident at 45° to excite the fluorescent particles in suspensions. A charge-coupled device (CCD) color camera system (VB-7010, Keyence, Japan) with a band-pass filter (580 ± 5 nm) was used to capture the emission signals from the sample at 60 s intervals. To avoid saturating the PL images, the laser intensity was adjusted by using a neutral density (ND) filter. The characteristic PL intensity was obtained from the maximum intensity of the Gaussian distribution with respect to the background PL at different drying times. A CCD beam profiler (Beam On, Duma Optronics, Ltd., Israel) was positioned on the side opposite of the laser to capture the 45° reflection and obtain the size and shape of the laser beam reflected from the coating. The captured image was analyzed by software (Beam On USB 2.0 measurement system, Duma Optronics, Ltd., Israel).

The 500-μm-thick suspension was cast onto the glass substrate by using a micropipette. Before coating, the glass surface was cleaned for 15 min in a vacuum by using a plasma etching device (Meiwafosis, SEDE-GE). The coated area was set at 25 cm^2 by gluing a 1.0-mm-thick duralumin shim onto the substrate. The substrate-bottom temperature was adjusted to 50 or 60 °C by using a heating plate (MD-10DMFH, Kitazato, Japan) placed beneath the coating at interspaces of 250 μm. Solvent loss was simultaneously measured in real time by using an electronic balance (Cubis MSE-3203S-0-00-DE, Sartorius, Japan) at a sampling rate of 1.0 Hz. All equipment was set up on a vibration isolation table and was covered with a black curtain to prevent exterior light from interfering with the measurements. A more detailed experimental procedure is given elsewhere [6]. The drying conditions and shear viscosities of the suspending medium were chosen so that $Pe > 10^3$ in order to ensure that the rate of film shrinkage was orders of magnitude greater than that of the Brownian diffusion of particles predicted by the Stokes–Einstein diffusion coefficient. We also estimated the rate balance between sedimentation and evaporation for the sedimentation number, $N_s = U/E$, where U is the Stokes' settling velocity. $N_s < 0.01$ falls within our experimental conditions of interest, indicating that the gravity-driven settling of latex particles is negligibly slow.

Optical model

We now describe the one-dimensional light absorption/emission model to predict the evolution in PL intensity from an evaporating bimodal suspension. Let us consider a top-down irradiation at λ = 532 nm with an exponential decay in intensity obeying the Beer's law. Assuming a uniform concentration of particles over a thin layer of thickness Δ*z*, the difference (Δ*I*) in intensity of pump light absorbed within the given layer is:

$$\log_{10}\frac{I+\Delta I}{I}=\sum_{\alpha=1,2}\varepsilon_{A\alpha}\phi_{\alpha}\Delta z\,. \qquad (1)$$

where I denotes the intensity of light that penetrates the layer, ε_A is the light absorption coefficient at the excitation wavelength of 532 nm, ant ϕ is the local volume fraction of particles. The subscript α = 1, 2 denotes the small (i.e., fluorescent) and large (i.e., nonemissive) particles, respectively.

The intensity of the 580 nm-emittance from the fluorescent particle is proportional to Δ*I*,

$$F=\Psi\Delta I\,. \qquad (2)$$

where the quantum yield (ψ) is assumed to be constant.

The emitted light is partly absorbed as it passes through the suspension because of the nonzero light absorption coefficients (ε_B) of the large and small latex particles at the emission wavelength. For a numerical prediction, we used N = 2000 nodes in the thickness direction to calculate the intensities of locally emitted and absorbed PL signals at each node. The PL signal emitted from *i*-th node reaches the liquid surface with the intensity F_i, which is expressed as,

$$\log_{10}\frac{F_i}{\Psi\Delta I_i}=-\sum_{j=1}^{i}\sum_{\alpha=1,2}\varepsilon_{B\alpha}\phi_{j\alpha}\Delta z \quad (3)\,.$$

where ΔI_i is the local intensity difference at *i*-th node. Combining local emissions at different depths, we obtained the overall intensity of PL emitted from the suspension surface, $F=\sum_{i=1}^{N}F_i$, and compared it with the results of experiment. A preliminary calculation shows that the increase in the number of nodes above 2000 does not significantly change the calculated emission intensity.

The volume fractions of particles vary as the suspension dries. For simplicity, we restricted ourselves to the case of *P*e >>1, in which the particle depth profile becomes discontinuous. The lower layer maintains the initial volume fraction of $\phi_{\alpha 0}$ (α = 1, 2) for each particle, whereas the upper layer, containing close-packed particles, has a higher but constant volume fraction of $\phi_{\alpha u}$. The packed-particle front recedes downward as the drying proceeds. Assuming that the small particles fill the interstitial space between the large particles, the packing layer thicknesses for small and large particles are obtained from the mass balance as follows:

$$d_1 = \frac{\phi_{10}}{(\phi_{1u} - \phi_{10})(1 - \phi_{2u})} Et \quad (4),$$

$$d_2 = \frac{\phi_{20}}{\phi_{2u} - \phi_{20}} Et \quad (5).$$

Results and Discussion

To begin, we predicted the PL dynamics by using the one-dimensional optical model for three suspensions with different distributions of large and small particles. Figure 2 shows the variation in PL intensity as a function of drying time, which is made dimensionless by the characteristic time scale h_0/E, where h_0 is the initial film thickness. The rate of film shrinkage is assumed to be constant at E = 0.4 μm/s. When the suspension contains a homogeneous distribution of particles (case A), the PL intensity remains constant and at its initial value until the drying completes. Conversely, the calculated PL intensity first decreases and then increases to reach unity when the large particles preferentially segregate on the top surface to show the random closed packing of ϕ_{2u} = 0.64, whereas the small particles are uniformly distributed (case B). The reduction in PL intensity early-on in the drying process stems from the cutoff of excitation and emission lights absorbed by the nonemissive large particles accumulating in the vicinity of the free surface. However, the opposing trend (i.e., a monotonic increase in intensity) emerges when both particles co-segregate to form a bimodal packing layer, in which the interstitial spaces between close-packed large particles are filled with the small latex particles (case C). The increase in the concentration of the fluorescent particles at the surface leads to greater PL, which overcomes the absorption and emission cutoff of the large, nonemissive particles, thereby increasing the PL intensity as the particles stratify.

To examine the drying-induced particle consolidation in a quantitative sense, we measured the PL dynamics and compared it with the theoretical predictions. Figure 3 shows a typical example of 580 nm PL as a function of drying time. The intensity is normalized by that of the initial intensity (i.e., just after coating). The evolution in PL intensity indicates a particular two-step segregation of fluorescent particles: the intensity gradually increases first but then undergoes a step-wise increase to a higher intensity at a certain drying time. Further drying results in no significant change in PL intensity. The simultaneous measurement of the film mass reveals a transition from the gas-diffusion-limited evaporation with a constant rate of mass loss toward the later stage with reduced drying rates. The secondary rise in PL intensity emerges during the latter period of evaporation, and completes within 60 s before the drying finishes. This transient emission is well reproduced by the numerical calculations. We use the mass-loss data to determine the initial film shrinkage rate E, and thus the consolidation layer thickness of each particle from Eqs. (4) and (5). Because the particle volume fractions in the consolidation layer are unknown, we assume a random close packing of large particles (ϕ_{2u} = 0.64), as per the literature [2], and insert the time-dependent volume fraction of small particles

(ϕ_{1u}) to achieve the best fit between the measured and predicted PL intensities. The estimated volume fraction increases slightly in the early evaporation period, then increases to $\phi_{1u} = 0.25$, which agrees well with the theoretical value of 0.23 for the case when the interstitial spaces between large particles are filled with the small particles in random close packing. These results imply that the secondary particle segregation is due to the transport of small particles toward the interstitial spaces near the free surface, which is consistent with the previous physical model [see Ref [3], and references therein].

To investigate what triggers the onset of secondary particle segregation, we analyzed the image analyses of the laser spot reflected from the surface of suspensions containing particles with various diameters. The diameter d_1 of the small particle is fixed at 100 nm, whereas that of the large particle (d_2) is either 8 μm or 200 nm. For $d_2/ d_1 = 80$, the onset time of the second migration agrees with that of the quick expansion of the beam spot, as depicted in Figure 4. Conversely, no significant increase in PL intensity appears for $d_2/ d_1 = 2$, although the beam expansion occurs as does for the larger ratio of particle size.

The onset of the expansion of the reflected beam is attributed to the invasion of the air-liquid interface into the consolidation layer of particles. At high Peclet numbers, the particle-consolidation front recedes as the packing layer grows and eventually reaches the substrate. Further evaporation causes a curve in the interface that meets the surfaces of neighboring particles. Subsequently, the particles protrude from the liquid surface as the interface retracts through the pores between the particles. The excitation beam scatters from either the deformed interfaces or from the particle surfaces, thereby expanding the beam spot at a certain drying time.

The meniscus invasion also causes a capillary pressure, which drives a convective motion of particles in the liquid. When the air-liquid interface meets the particle surface at a contact angle of $\theta < 90°$, the concave interfacial profile between the neighboring particles leads to a lower liquid pressure beneath the meniscus, which generates a pressure-driven flow toward the free surface that transports the small particles through interstitial pore spaces between the large particles [3]. This scenario is consistent with our observations that the secondary increase in PL intensity diminishes at the low particle size ratio. For hexagonal packing of monodisperse particles with a diameter d_2, the pore-throat diameter is $0.15d_2$ [3]. A small particle with a diameter of d_1 can thus pass through the pore throat when $d_2/ d_1 > 7$. In the present case of $d_2/ d_1 = 2$, the convective transport of the small particles may be blocked by the large particles, leading to show negligible surface segregation of the small particles.

To verify this hypothesis, we predicted the time scale for the convective particle transport by assuming a flow in a pipe of diameter d_1. Consider the laminar flow of a Newtonian fluid with viscosity μ, and surface tension σ. When the capillary pressure 2σ/r drives the flow of fluid along the thickness h, the velocity of fluid is $v = (2\sigma / r)d_1^{\,2} / (32\mu h)$, where the radius of curvature, r, is assumed to be given by $r = d_1/2$. Inserting the average viscosity at the onset time of light scattering, we

obtained $v = 3.6\ \mu m/s$, and the corresponding time scale for fluid motion is $h/v \sim 6\ s$.The shorter time scale relative to our measurement time interval of Δt = 60 s implies that the flow is fast enough to transport the particles toward the free surface within Δt, which is consistent with the stepwise increase in PL intensity.

From a practical viewpoint, a suppressed migration of particles is often preferred to achieve uniform coatings. We expect that the increase in suspension viscosity could hinder the convective motion, and thus the secondary segregation of small particles, if the pressure-driven flow plays a role. To check this, we explored how the effect of initial polymer concentration affects the transient PL emission. The two-step increase in PL intensity appears at low CMC concentrations (Figure 5a), whereas the PL emission remains almost constant until the onset of the stepwise increase in PL intensity at high CMC concentrations (Figure 5c). In a particular intermediate range of polymer concentrations, the emission intensity initially remains constant but then increases and eventually rises quickly to a higher level at a certain drying time (Figure 5b). The final PL intensity after the secondary "jump" monotonically decreases with increasing the CMC concentration, which provides a direct evidence that an increase in viscosity tends to suppress the surface segregation of small particles. However, it is not immediately clear why the first rise in intensity diminishes with increasing the polymer concentrations. As mentioned above, our model predictions indicate that a higher viscosity (i.e., higher *P*e) gives rise to a monotonic increase in PL intensity due to the co-segregation of small and large particles at the free surface (see Figure 2), showing a qualitative disagreement with the measurements. The PL intensity may remain constant when excessively high polymer concentrations induce the entanglement of polymer chains, which could trap the particles and thereby retain the homogeneous distributions; however, this physical picture is not sufficient to explain the subsequent slowly increasing intensity in the later drying stage. In a future study, we plan to elucidate how the polymer chains interact with suspended particles to suppress their surface segregation.

Conclusions

We used *in-situ* photoluminescence (PL) microscopy to investigate the preferential migration of small fluorescent latex particles co-dispersing with large nonemissive latex particles in an aqueous polymer solution. The measurements reveal a two-step migration of fluorescent particles: a slow primary segregation is followed by a secondary, stepwise segregation, which emerges when the air-liquid interface invades into the particle consolidation layer. The secondary segregation is attributed to a flow-induced motion of small particles that move through interstitial spaces between large particles. We develop a one-dimensional optical emission-absorption model to predict the transient PL intensity. Good consistency between the measured and predicted PL intensities allows us to quantify the dynamical particle distribution.

Acknowledgement

We acknowledge the financial support of the Japan Society for the Promotion of Science (JSPS) KAKENHI (26420766) Grant-in-Aid for Scientific Research C.

References

[1] Cardinal, CM, Jung, YD, Ahn, KH, Francis, LF, "Drying regime maps for particulate coatings", *AIChE J.*, 56, 2769-2780 (2010)

[2] Routh, AF, Zimmerman, WB, "Distribution of particles during solvent evaporation from films", *Chem Eng Sci.*, 59, 2961–2968 (2004)

[3] Luo, H, Cardinal, CM, Scriven, LE, Francis, FL, "Ceramic nanoparticle/monodisperse latex coatings", *Langmuir*, 24, 5552-5561 (2008)

[4] Nikiforow, I, Adams, J, Koenig, M, Langhoff, A, Pohl, K, Turshatov, A, Johannsmann, D, "Self-stratification during film formation from latex blends driven by differences in collective diffusivity", *Langmuir*, 26, 13162-13167 (2010)

[5] Atmuri, AK, Bhatia, SR, Routh, AF, "Auto-stratification in drying colloidal dispersions: effect of particle interactions", *Langmuir*, 28, 2652-2658 (2012)

[6] Lim, S, Ahn, KH, Yamamura, M, "Latex migration in battery slurries during drying", *Langmuir*, 29, 8233-8244 (2013)

[7] Trueman, RE, Domingues, EL, Emmett, SN, Murray, MW, Keddie, JL, Routh, AF, "Auto-stratification in drying colloidal dispersions: experimental investigations", *Langmuir*, 28, 3420-3428 (2012a)

[8] Tzitzinou, A, Keddie, JL, "Film formation of latex blends with bimodal particle size distributions: consideration of particle deformability and continuity of the dispersed phase", *Macromolecules*, 33, 2695-2708 (2000)

[9] Buss, F, Roberts, CC, Crawford, KS, Peters, K, Francis, LF, "Effect of soluble polymer binder on particle distribution in a drying particulate coating", *J. Colloid Interface Sci.*, 359, 112-120 (2011)

[10] Trueman, RE, Domingues, EL, Emmett, SN, Murray, MW, Routh, AF, "Auto-stratification in drying colloidal dispersions: A diffusive model", *Journal of Colloid and Interface Science*, 377, 207-212 (2012b)

[11] Hagiwara, H, Suszynski, WJ, Francis, LF, "A Raman spectroscopic method to find binder distribution in electrodes during drying", *Journal of Coatings Technology and Research*, 11(1), 11-17 (2014)

[12] Jaiser, S, Muller, M, Baunach, M, Bauer, W, Scharfer, P, Schabel, W, “Investigation of film solidification and binder migration during drying of Li-Ion battery anodes”, *Journal of Power Sources*, 318, 210 -219 (2016)

List of Figures

Figure 1 Experimental setup

Figure 2 Time-evolutions in PL intensities predicted from the one-dimensional optical model in cases of (A) homogeneous particle distributions, (B) preferentially surface segregation of large particles, and (C) co-segregation of small/large particles to form a bimodal packing layer. The film shrinkage rate is E = 0.4 μm/s. Initial particle fractions are 2.8 vol% and 0.4 vol% for large and small particles, respectively. The initial film thickness is 500 μm. The particle volume fractions in the consolidation layer satisfy ϕ_{2u} = 0.64 in cases (B) and (C), and ϕ_{1u} = 0.23 in case (C).

Figure 3 Variations in the PL intensity and film mass with drying time. The emission shows two-step increase in intensity at different drying times. The predicted emission intensity agrees with measurements. The initial particle fractions are 2.91 vol% and 0.41 vol% for large and small particles, respectively. The initial polymer concentration is 0.5 wt%. The substrate temperature is 50 °C.

Figure 4 Time-variations in (a) PL intensity and (b) spot diameter of beam reflected from the liquid surface at different diameters of large particles. No significant increase in PL intensity was observed at the size ratio of large-small particle diameters of d_2/ d_1 = 2. The initial particle fractions are 1.5 vol% and 0.2 vol% for large and small particles, respectively. The initial polymer concentration is 0.5 wt%. The substrate temperature is 50 °C.

Figure 5 Time-evolutions in the measured PL intensities at different initial CMC concentration of (a) 0.3 wt%, (b) 0.5 wt%, and (c) 0.7 wt%. The final emission intensity reduces, whereas the primary increase in emission intensity diminishes, as increasing the polymer concentration. The initial particle fractions are 2.91 vol% and 0.41 vol% for large and small particles, respectively. The substrate temperature is 50 °C.

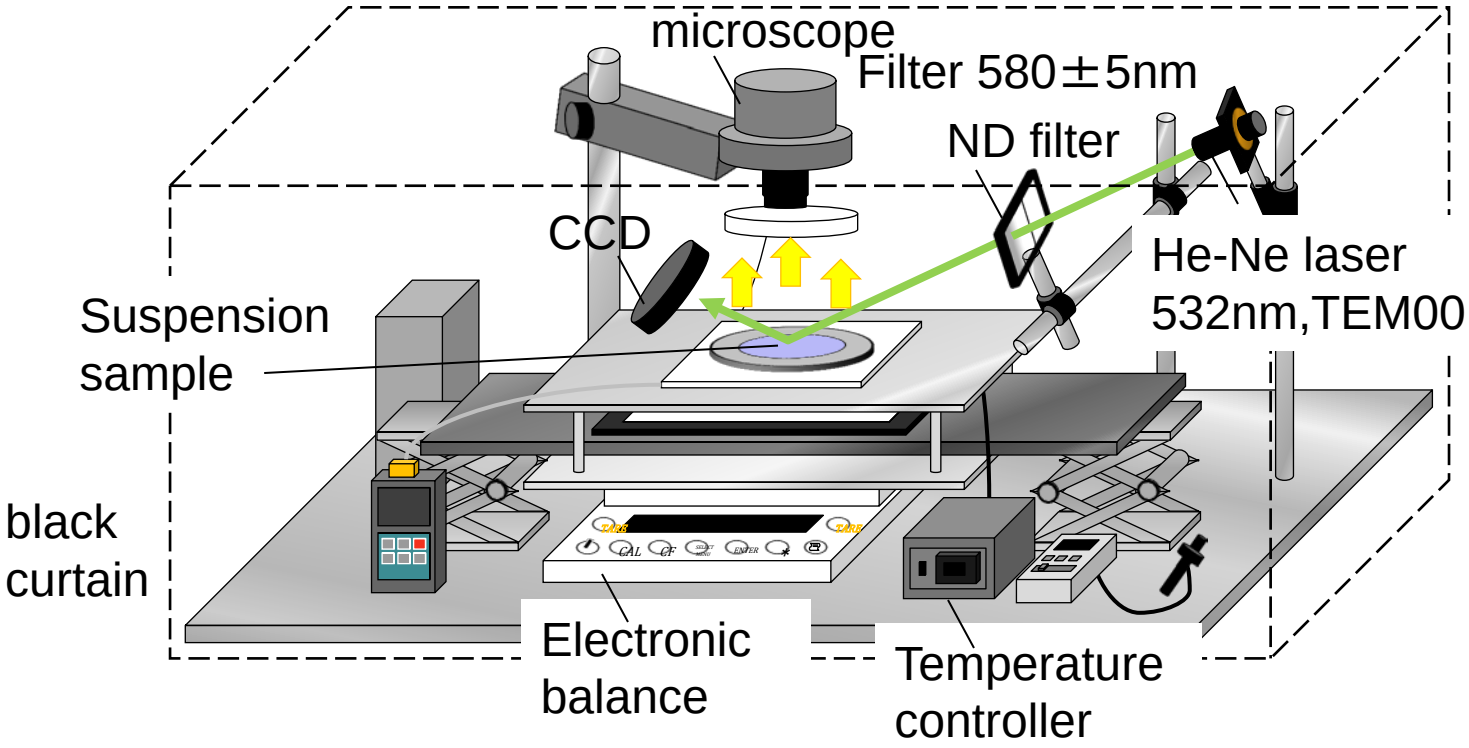
microscope
Filter 580±5nm
ND filter
CCD
He-Ne laser
532nm,TEM00
Suspension
sample
black
curtain
Electronic
balance
Temperature
controller

Figure 1

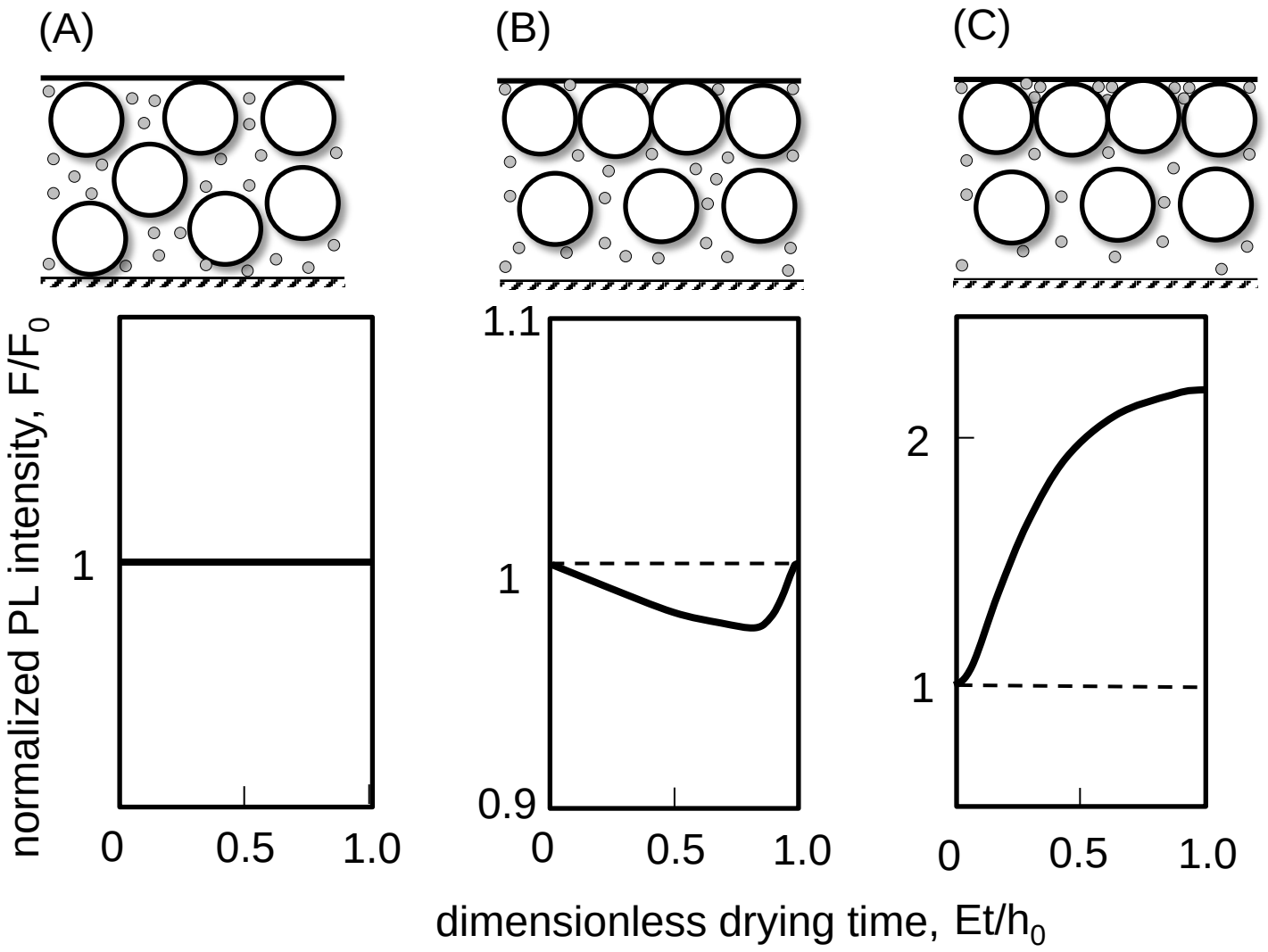
(A)
(B)
(C)
normalized PL intensity, F/F0
1
1.1
1
0.9
2
1
0
0.5
1.0
0
0.5
1.0
0
0.5
1.0
dimensionless drying time, Et/h0

Figure 2

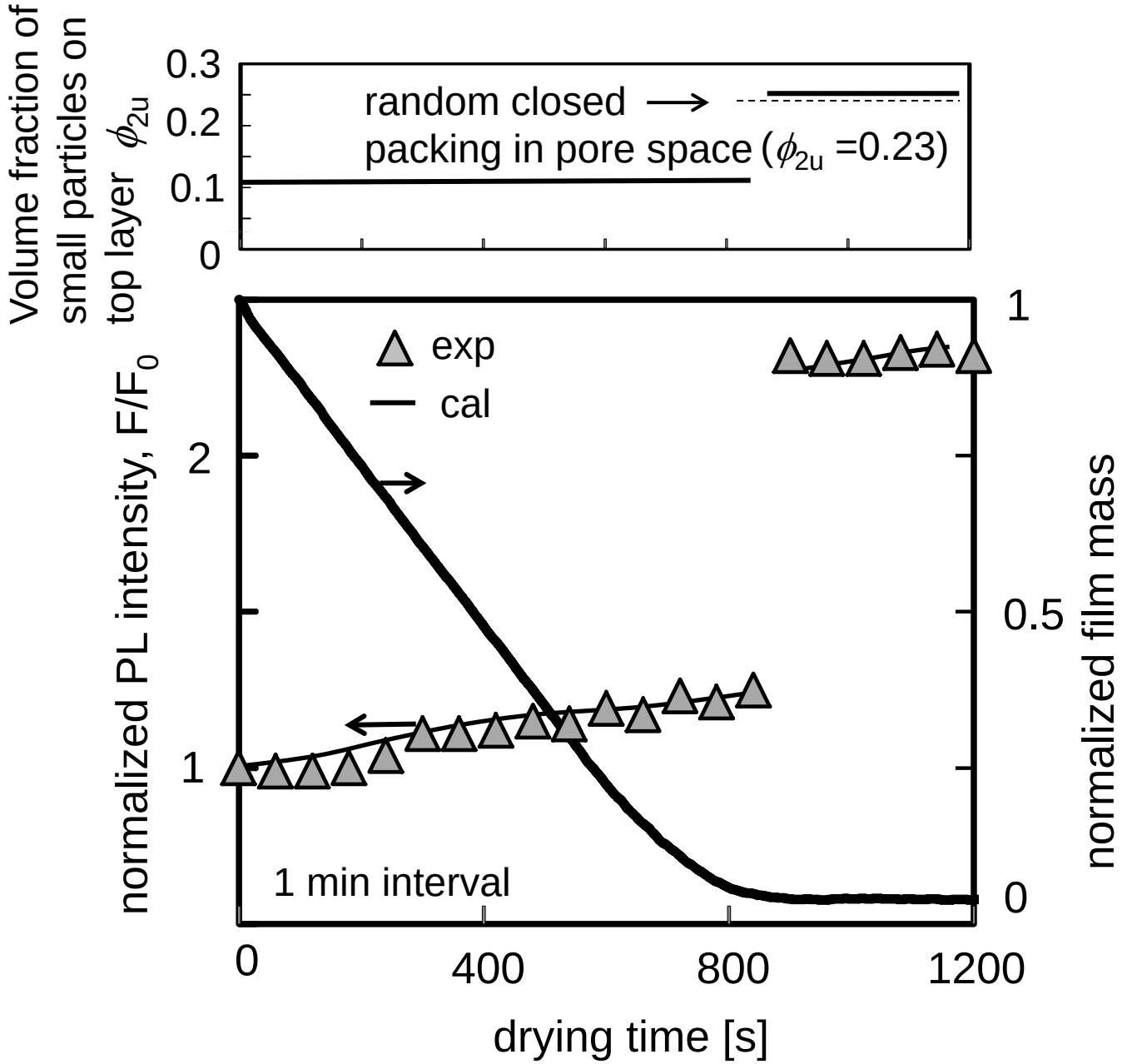
Volume fraction of small particles on top layer ϕ_{2u}
0.3
0.2
0.1
0
random closed packing in pore space (ϕ_{2u} =0.23)
exp
cal
normalized PL intensity, F/F$_0$
2
1
1 min interval
1
0.5
0
normalized film mass
0
400
800
1200
drying time [s]

Figure 3

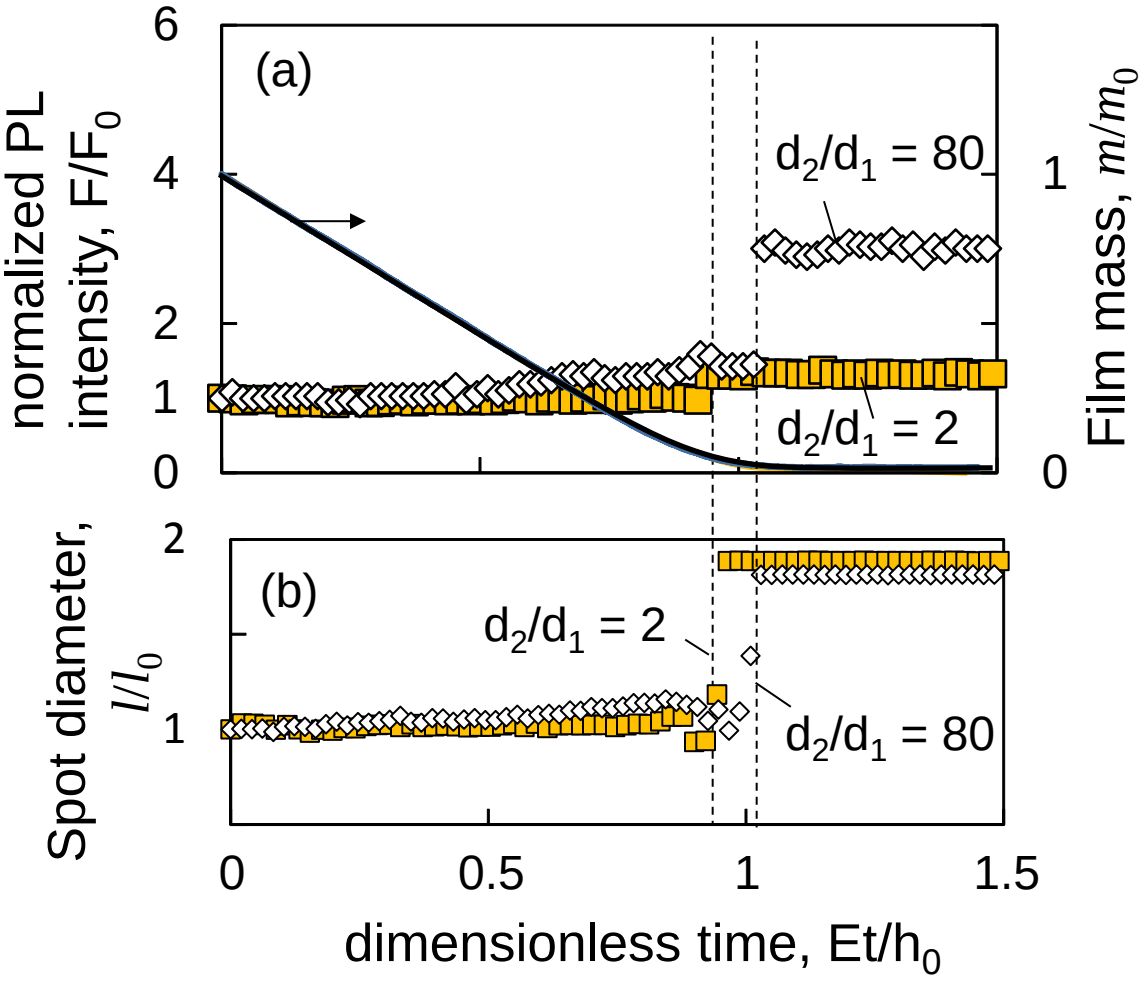
(a)
(b)
normalized PL intensity, F/F0
Film mass, m/m0
Spot diameter, l/l0
d2/d1 = 80
d2/d1 = 2
d2/d1 = 2
d2/d1 = 80
6
4
2
1
0
1
0
2
1
0
0.5
1
1.5
dimensionless time, Et/h0

Figure 4

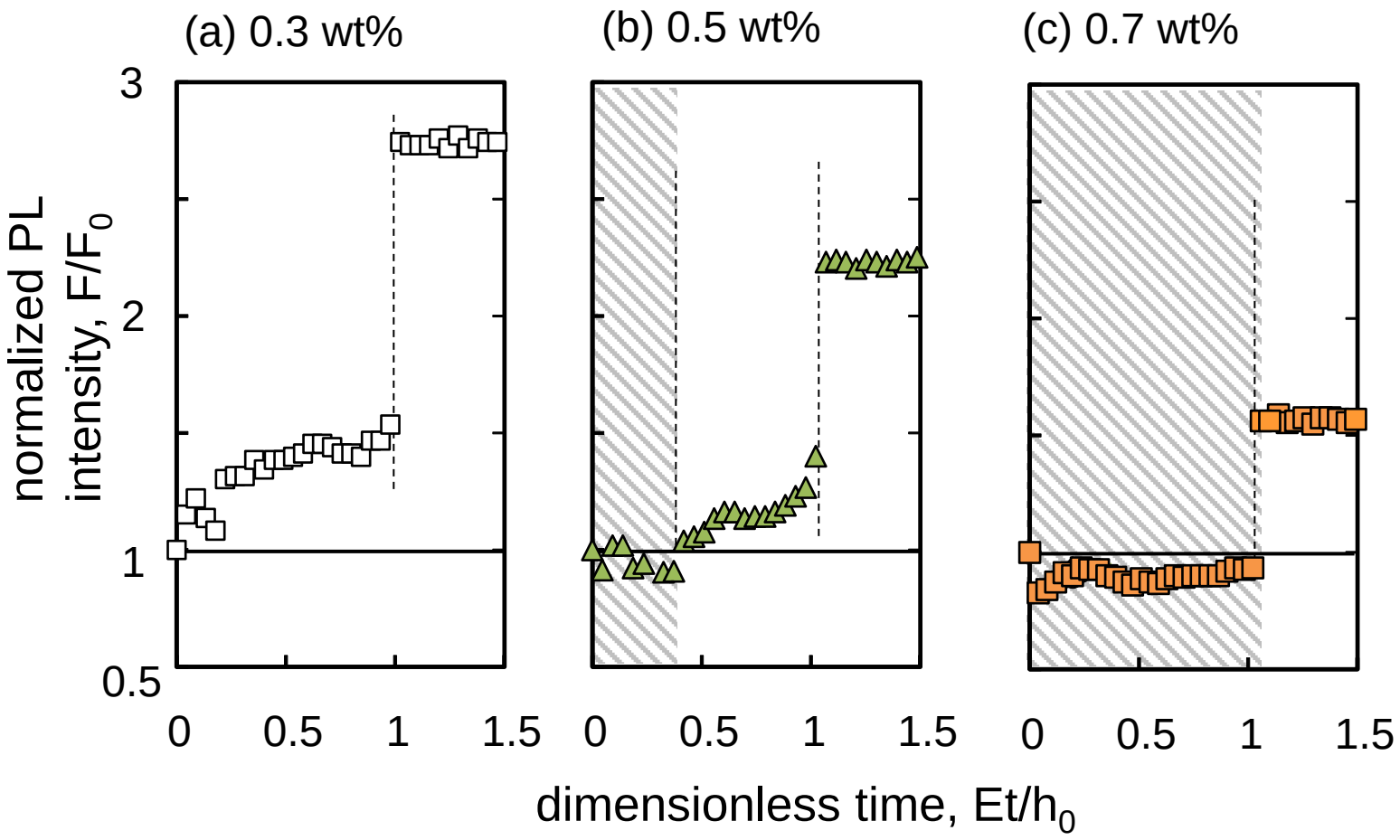
(a) 0.3 wt%
(b) 0.5 wt%
(c) 0.7 wt%
normalized PL intensity, F/F0
dimensionless time, Et/h0
3
2
1
0.5
0
0.5
1
1.5

Figure 5